Earth and Planetary Science Letters 603 (2023) 117984

Contents lists available at ScienceDirect

Earth and Planetary Science Letters

journal homepage: www.elsevier.com/locate/epsl

Estimating the 3D structure of the Enceladus ice shell from Flexural and Crary waves using seismic simulations

Angela G. Marusiak [a,*], Saikiran Tharimena [a,1], Mark P. Panning [a], Steven D. Vance [a], Christian Boehm [b], Simon Stähler [b], Martin Van Driel [c]

[a] Jet Propulsion Laboratory, California Institute of Technology, Oak Grove Drive, Pasadena, CA, 91109, USA
[b] ETH Zurich, Sonneggstrasse 5, Zurich, 8092, Switzerland
[c] Carl Zeiss SMT GmbH, Carl-Zeiß-Promenade 10, Jena, 07745, Germany

ARTICLE INFO

Article history:
Received 26 September 2022
Received in revised form 22 December 2022
Accepted 27 December 2022
Available online 12 January 2023
Editor: R. Bendick

Keywords:
seismology
surface waves
glaciation

ABSTRACT

A seismic investigation on Saturn's moon Enceladus could determine the thickness of the ice shell, along with variations from the mean thickness, by recovering phase and group velocities, and through the frequency content of surface waves. Here, we model the Enceladus ice shell with uniform thicknesses of 5 km, 20 km, and 40 km, as well as with ice topography ranging from 5-40 km. We investigate several approaches for recovering the mean ice shell thickness. We show that surface wave dispersions could be used to determine the mean ice shell thickness. Flexural waves in the ice only occur if the shell is thinner than a critical value < 20 km. Rayleigh waves dominate only in thicker ice shells. The frequency content of Crary waves depends on the ice shell thickness.

1. Introduction

Saturn's moon Enceladus has the best characterized ocean of the many discovered ocean worlds (Hendrix et al., 2018; National Academies of Sciences Engineering and Medicine, 2022), and is a high priority target for future exploration. Planned and studied missions to land on Titan (Barnes et al., 2021), Enceladus (Mackenzie et al., 2021), and Europa (Hand et al., 2017) include seismic payloads, similar to the seismic experiment on the InSight mission to Mars (Lognonné et al., 2019). Tidally flexed ocean worlds are anticipated to provide abundant seismic data that will be important for revealing internal mechanical and thermal structure (Kovach and Chyba, 2001; Pappalardo et al., 2013; Marusiak et al., 2021; Vance et al., 2021b,a). These constraints are needed to determine whether subsurface oceans are or were habitable (Vance et al., 2018). Better constraints on the ice shell structure provide the geophysical context for the potential subsurface environment. Sources of seismicity can provide context on the dynamics of the ice shell and ocean (e.g. Collins et al. (2022)). The main source of seismicity is likely tidal flexing (Hurford et al., 2020), with additional possible source including hydrothermal or volcanic activity at the base of the ocean (Waite et al., 2017; Choblet et al., 2017), and fluid motions as material is exchanged between the surface, ice shell, and ocean. Here, we investigate different approaches and methods for constraining the ice shell thickness of Enceladus using seismology. Previous studies (e.g. (Lee et al., 2003; Stähler et al., 2017; Maguire et al., 2021)) have focused on using simple one-dimensional modeling. However, the Cassini mission provided evidence for spatial variability in the thickness of the Enceladus ice shell, particularly with latitude (Iess et al., 2014; McKinnon, 2015; Čadek et al., 2016; Beuthe, 2018) (Fig. 1a). Due to its small radius of 252 km, surface waves on Enceladus can easily orbit the moon multiple times within $\leq$800 s. Rayleigh waves with wavelengths less than the ice shell thickness show little dispersion and will travel with speeds equal to 0.92 the shear wave velocity (Vs) (Kovach and Chyba, 2001). Flexural surface waves—those with wavelengths greater than the thickness of the ice—perturbed by the base of the ice shell will travel as full layer waves. These waves have intrinsic dispersion that depends on the velocity gradient in the ice (Panning et al., 2006; Stähler et al., 2017). It is expected that thin ice shells will cause Flexural waves to dominate the seismic records (Kovach and Chyba, 2001; Panning et al., 2006; Stähler et al., 2017; Maguire et al., 2021). In addition to Flexural waves, we anticipate to observe Crary waves (Crary, 1954). Crary waves (Cr) are monochromatic trapped waves that have a phase velocity equivalent to compressive velocities (Vp) and have characteristic harmonic frequency spectra (Equation 1) dependent on the ice shell thickness. The frequency content of the Crary wave spectrum along with the dispersion of surface waves and the tran-

* Corresponding author.
E-mail address: angela.marusiak@gmail.com (A.G. Marusiak).
[1] Now at Schibsted ASA, Akersgata 55, Oslo, 0180, Norway.

https://doi.org/10.1016/j.epsl.2022.117984

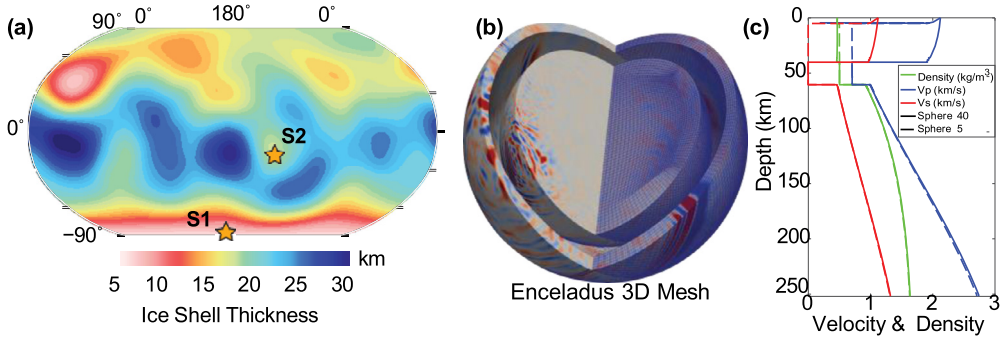

Fig. 1. Interior structure of Enceladus based on (Čadek et al., 2016) (see Methods). a) The ice shell thickness is allowed to vary laterally, with thinnest ice at poles and thickest ice near the equator. Two possible source locations (S1 and S2) are shown. b) The associated 3D mesh used to model the full seismic waveforms. Colors represent motion from a simulated encelaquake. c) Representative internal structures and wave velocities in 1D cross-section. (For interpretation of the colors in the figure(s), the reader is referred to the web version of this article.)

sition of Rayleigh to Flexural waves can be used to determine the ice shell thickness (Stähler et al., 2017).

2. Methods

We build one-dimensional models with uniformly thick ice shells of 5, 20, and 40 km (Olgin et al., 2011; Čadek et al., 2016; Lucchetti et al., 2017; Běhounková et al., 2017; Čadek et al., 2019) (Fig. 1a), and one model with topography built into the ice shell such that the thickness varies laterally ranging from 5 to 40 km allowing for more realistic 3D simulations (Fig. 1b). We use PlanetProfile (Vance et al., 2018, 2022) to generate geophysically-consistent interior structure models of Enceladus including the physical and bulk properties (Fig. 1c). PlanetProfile calculates geophysically consistent radial models, and calculates the seismic profile based on the SeaFreeze library (Journaux et al., 2020). PlanetProfile has been previously used to model seismic responses for Europa (Panning et al., 2018; Marusiak et al., 2022a), Titan (Marusiak et al., 2022b), and icy ocean worlds in general (Stähler et al., 2017). We maintain the same silicate, ocean and ice compositions for each of the models to maintain consistency, though the composition beneath the ice shell is somewhat arbitrary as we focus on the seismic wave propagation in the ice shell. We assume the ice shell is composed of pure water ice Ih for simplicity. Once we have the basic one-dimensional models, we extrapolate the results to create a three-dimensional model with laterally varying ice shell thickness. The ice surface topography is derived from measurements using Cassini's laser altimeter (Tajeddine et al., 2017). The ice-ocean boundary topography is derived from gravity data (Čadek et al., 2016, 2019). The interior structure models from PlanetProfile are used as inputs to create synthetic waveforms.

We create the synthetic waveforms using the Salvus software from Mondaic (Afanasiev et al., 2019). Our meshes (Fig. 1b) have a global resolution of 5 s and 3 s allowing us to incorporate the variations in ice shell thickness. We use Salvus to create models with 5 km, 20 km, 40 km thick ice, as well as a global model with varying ice shell thickness. Our source is a Mw 3.4, double-couple source (S1) as well as a real moment tensor from Lake Tanganyika (GMCTID: C201702240032A) (S2) scaled to be a Mw 3.4. Both were set at a depth of 3 km, within the ice shell. We set receivers to be globally located and spaced 1° apart. The magnitude of the source is somewhat irrelevant because we do not add background noise to our seismograms, meaning any size event would have high signal-to-noise ratios. Based on Hurford et al. (2020), who estimated seismic responses from tidal forces alone, a Mw 3.4 could be observed roughly once every ten tidal cycles, or roughly 14 earth days.

We set the seismograms to be 2000 s in length, which allows us to capture Flexural waves and Rayleigh waves that travel along major arcs (R1), minor arcs (R2), and multiple times around Enceladus (Rn) (Fig. 2).

3. Results

The ground motion and seismic responses for different ice shell models will reveal which approaches and seismic waves best constrain ice shell thickness.

3.1. Time-series analysis

Fig. 2 shows example seismic records of ground displacement for the different models. The source occurs at (-17°, 218°) and the receiver is about 160° away at (20°, 60°). The Rayleigh waves are easily identifiable on the thicker and variable thickness models. By contrast, the Flexural wave is best seen with thin or variable thickness models. Because the thickness of the ice is greater than the wavelength of the surface waves, the Flexural wave is not visible for thick ice, and its absence allows for the R3 and R4 Rayleigh waves to be revealed. The Flexural wave does not disappear entirely, but the period at which it dominates becomes increasing long, thus more difficult to observe. Including ice shell topography allows both R1, R2, and Flexural waves to be seen, but the seismograms do have more dispersive energy, producing weaker ground motions compared to uniform ice shells. In the model with topography, the mean ice shell thickness is about 20 km, which allows both the Rayleigh and the Flexural waves to be observed. The Flexural wave is particularly strong, and stronger than a uniform 20 km ice shell.

The differences in seismic phases are further revealed by examining the moveout of key seismic phases in distance and time (Fig. 3). Including under-ice topography tends to reduce amplitudes compared to models with uniform ice shell thickness. The thinner ice shell has stronger motion in the horizontal component for events within $\approx 50°$ of the receiver. This short separation can obscure some of the body phases, including reflections off the ice shell (e.g. SeS, SeP, PeP, see Stähler et al. (2017)) that are more easily observable on thicker ice shells, or in models with surface topography. The ice shell reflections could be used to determine the thickness of the ice shell at the points of reflection, providing additional data to constrain the average ice shell thickness. If the locations of multiple seismic events are well constrained, the recovered ice shell thicknesses from the ice reflections could be used to map variations in the ice shell thickness.

3.2. Surface wave dispersion

The spectra of seismograms also highlight differences among the models (Fig. 4). For each model we create a filtered, Gaus-

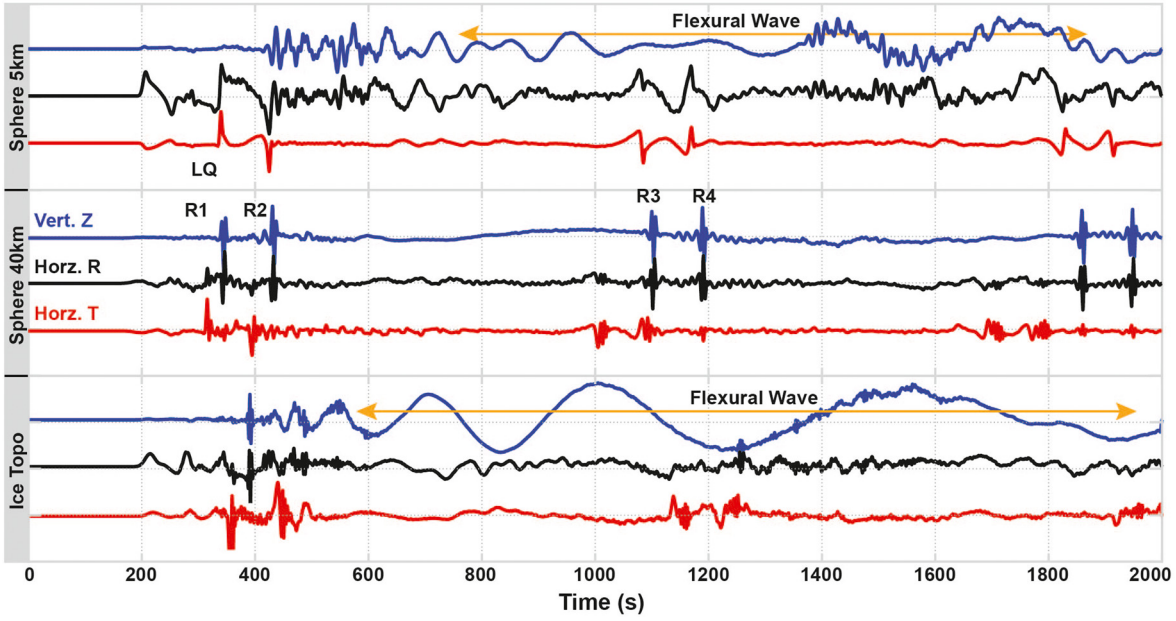

Fig. 2. Ground motions in the vertical (blue), horizontal radial (black) and horizontal transverse (red) directions for an event with a depth of 3 km, Mw 3.4, and the moment tensor from the Lake Tanganyika event. The receiver is set at an epicentral distance of 160°. The ground displacement normalized to the maximum value is shown for a 5 km (top), 40 km (middle), and variable ice thickness (bottom) models. Key surface waves such R1, R2, R3, and R4 are labeled. The Flexural wave (orange arrows) is shown for the thin and variable thickness models.

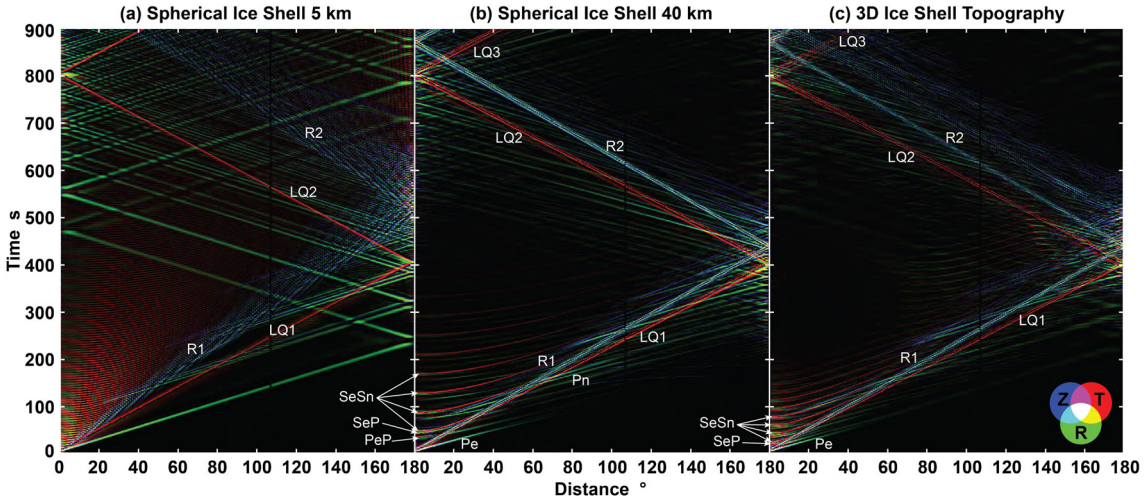

Fig. 3. Ground motions in the vertical (blue), horizontal radial (green) and horizontal transverse (red) directions for an event with a depth of 3 km, Mw 3.4, and the moment tensor from the Lake Tanganyika event. Time (s) is plotted on the y-axis, epicentral distance (°) on the x-axis, and the intensity of the color indicates the amount of ground displacement recorded on the three components. White indicates strong motion on all three components. Panels show resulting ground displacements for ice shell thicknesses of a) 5 km, b) 40 km, and c) for variable ice shell thickness.

sian envelope around a centered frequency. Each tapered envelope (Fig. 4e, red) is represented by a row in Fig. 4a-d, to highlight the modes of the Rayleigh waves and Flexural wave. The Flexural wave is more clearly visible in models with thin ice shells and has the strongest signal. In thicker ice shells, the Flexural wave is not clearly seen, however the Rayleigh waves are identifiable. Rayleigh waves dominate at periods between 5-20 s. In the model with ice topography, the transition is seen between Rayleigh and Flexural waves at periods of $\geq$ 20 s. It is worth noting, that although the model with ice topography (Fig. 4 d) has a mean ice shell thickness of 20 km, there are clear differences from the model with uniform 20 km ice thickness (Fig. 4 b). In particular, the model with ice topography shows the Flexural wave present for longer durations of time at longer period ($>$ 200 s) compared with the uniform model.

We show that our picked group velocities match those predicted by the Mineos software package (Masters et al., 2011) for periods greater than $\approx$ 20 s for the 5 km uniform ice shell (Fig. 5). In our model with ice topography, the group velocities are close to the dispersion curve for a 20 km ice shell. This result is not surprising, as the mean ice shell thickness was 17-20 km depending on the receiver location. For the thinner 5 km ice shell, the group velocity is about 1.5 km/s for periods less than 20 s. For the model with under-ice topography, the group velocity is about 1.5 km/s for periods less than $\approx$ 75 s. The results indicate that group velocities can be used to recover mean ice thickness for given travel paths.

Crary waves can also constrain the ice shell thickness. We use the spectra for a window of time surrounding the Crary wave arrival to compare the differences among the models. We calculate the frequency of the Crary wave f_{CR} by assuming a Vp value of 3.9 km/s, and a Vs value of 1.97 km/s (Equation (1)). These velocities are used to predict the arrival time of the Crary wave. The charac-

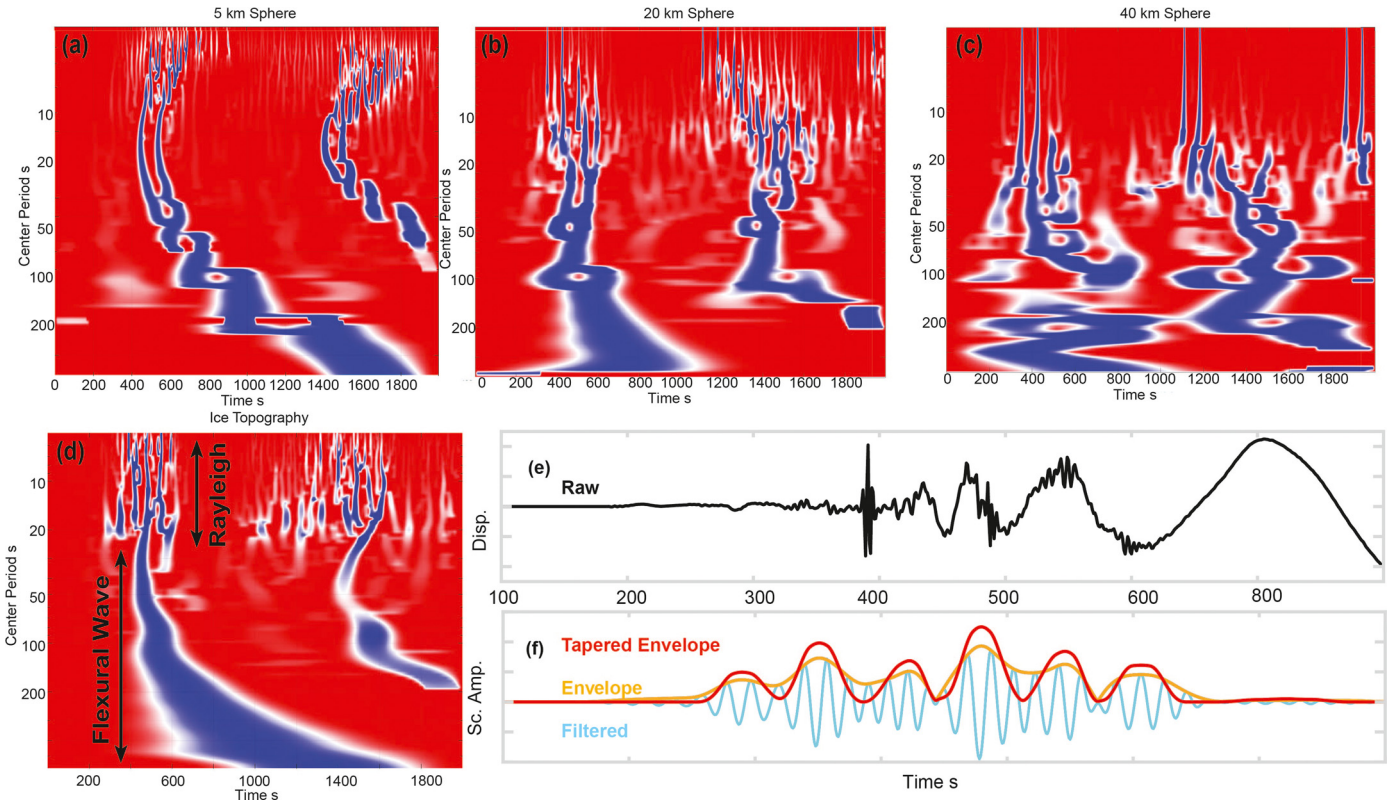

Fig. 4. An event occurring at a distance of 160°. The filtered and tapered envelopes of models with uniform ice shell thicknesses of a) 5 km, b) 20 km, c) 40 km, and d) the model with ice topography are vertically stacked in order to highlight the dispersion of the surface waves for given center periods. The spectra are created by taking raw seismograms (e, black) using a narrow band Gaussian bandpass filter (centered at 17.8 s in this example) (f, cyan), and then computing envelopes of energy packets to estimate the dispersion of the surface waves (f, orange). The tapered envelope (f, red) helps to separate phases that may occur close in time see Fig. 3) and is used to create stacks (a-d) based on time (x-axis) and center period (y-axis).

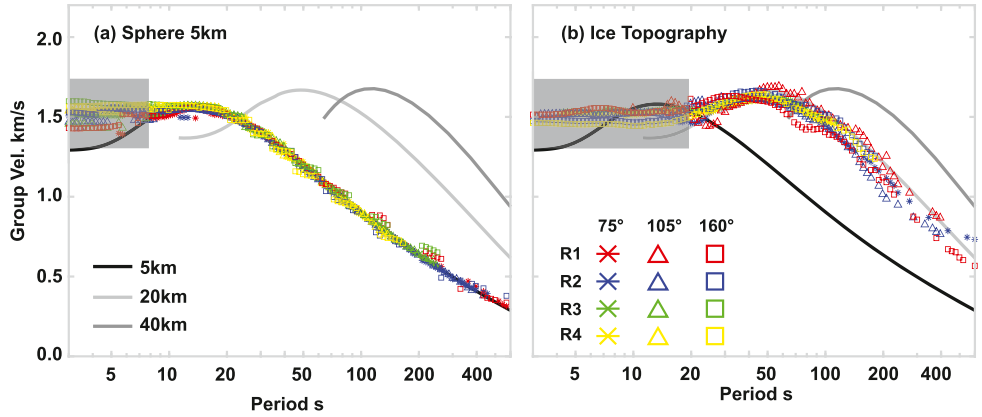

Fig. 5. Group velocities for 3 receivers at 75° (cross), 105° (triangle), and 160° (square) from the source, computed using the dispersion curves in Fig. 4. Solid curves represent the group velocity curves for 5 km (black), 20 km (light gray), and 40 km (dark gray) ice shell models. a) The dispersion curves for a 5 km thick ice shell. b) Model with ice topography. The mean ice shell thickness is 20 km, 19 km, 18 km, and 17 km thick for receivers R1 (red), R2 (blue), and R3 (green), and R4 (yellow) respectively. The shaded gray box indicates where the recovered group velocities vary from the theoretical group velocities.

teristic frequency (when $n = 1$) and the overtones (when $n > 1$ and an integer) are strongly dependent on the thickness of the ice shell (d). The predicted Crary wave frequencies are shown as dashed green lines in Fig. 6. Thin ice shells (< 20 km) match the predicted resonant frequencies, but the thicker ice don't necessarily show strong peaks everywhere they were predicted. Furthermore, the model with variable ice shell thickness produces periodograms similar to, but not matching exactly, the model with a uniform 20 km ice shell just as the stacked spectra showed there are differences between a model with uniform 20 km ice shell thickness and a model with a mean ice shell thickness of 20 km that has topography. If recovered Crary wave periodograms from future missions likewise fail to fit a model with uniform thickness, we can estimate the mean ice shell thickness and infer there is some topography.

$$f_{Cr} = \frac{(n+1)Vs}{2d\sqrt{1 - \frac{Vs}{Vp}^2}} \quad (1)$$

4. Discussion

We investigate different approaches for recovering the ice shell thickness from several models. By creating one model with ice to-

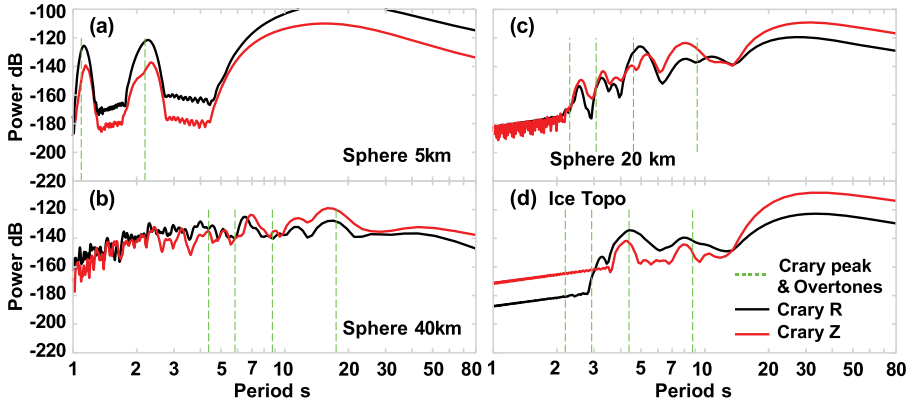

Fig. 6. Periodograms of the vertical (red) and radial (blue) components for models with ice shell thickness of a) 5 km, b) 40 km, c) 20 km and d) with ice topography. A time window was applied surrounding the predicted Crary wave arrival. Dashed green vertical lines represent the calculated frequencies for Crary waves using Equation (1).

pography, thus variable ice shell thickness, we can better compare which methods can be used to recover mean ice shell thickness. We show that the presence, or lack thereof, of Flexural waves and Rayleigh waves can indicate relative thickness of the ice shell. Depending on the source-to-receiver distance and the thickness of the ice shell, we anticipate different waves should dominate the seismic records. Thinner ice shells will show strong Flexural waves, but may obscure reflected body waves. Thicker ice shells are more likely to produce strong Rayleigh waves and allow for the observation of more body waves (depending on distance from the event). Body waves, including reflections off the ice-ocean interface, could be used to infer the thickness of the ice shell at the bounce point. The use of surface waves dispersions will likely yield the thickness of the ice shell. This finding is consistent with previous studies on Europa (Maguire et al., 2021) that also explore the role of surface wave dispersion for recovering ice shell thickness. We show that the frequency content and group velocity of the surface waves will reveal the mean ice shell thickness along the travel path from the source to receiver. For a model with variable ice shell thickness, comparisons of dispersion from different events could indicate regions, or least the relative directions, where the ice varies from the mean thickness.

If a seismometer is sent to Enceladus, the data will likely be affected by several sources of uncertainty which we do not model here. In this study we do not add any background noise and we know precisely when and where the events are occurring. Some uncertainty in the timing and location of the seismic events should not greatly affect our analysis. Unlike body waves, whose arrival times need to be known precisely, surface wave dispersion calculations don't heavily rely on timing. However, in order to better determine where the ice shell does vary on a regional or global scales, the travel paths of the surface waves need to be known. Background noise could cause uncertainty in our analysis, as it would decrease the overall quality and signal-to-noise ratio of the event. Modeling anticipated background noise is beyond the scope of this study. It is worth repeating that the Mw 3.4 events we use could be caused by tidal forces (Hurford et al., 2020) and could occur about every two earth weeks. Such seismicity would likely be detectable by future landed missions such as the Enceladus Orbilander (Mackenzie et al., 2021), but the detection limits would depend on the specifications of the seismic instrument. We also assume there is no porosity, which limits scattering effects. Strong scattering could obscure surface waves making our analysis more challenging. If attenuation is stronger than anticipated, we may detect fewer events and the detected events would have weaker signal strength due to reductions in ground motion.

5. Conclusion

We show that time-series and spectral analysis of surface waves can recover mean ice shell thickness for the icy-ocean world, Enceladus. Our model with variable ice shell thickness included both Rayleigh and Flexural wave arrivals. The frequency content of these waves can be used to constrain mean ice shell thickness. The dispersion curves for these waves can further indicate the mean ice shell thickness along the travel path of the seismic waves.

CRediT authorship contribution statement

Angela G. Marusiak: Data curation, Investigation, Visualization, Writing – original draft, Writing – review & editing. **Saikiran Tharimena:** Conceptualization, Formal analysis, Investigation, Methodology, Software, Visualization, Writing – review & editing. **Mark P. Panning:** Conceptualization, Methodology, Resources, Supervision, Writing – review & editing. **Steven D. Vance:** Funding acquisition, Project administration, Resources, Supervision, Writing – review & editing. **Christian Boehm:** Writing – review & editing. **Simon Stähler:** Methodology, Writing – review & editing. **Martin Van Driel:** Writing – review & editing.

Declaration of competing interest

The authors declare that they have no known competing financial interests or personal relationships that could have appeared to influence the work reported in this paper.

Data availability

Raw seismograms and mineos results are available on Zenodo (doi: 10.5281/zenodo.7023774, https://zenodo.org/record/7023774#.Yw0cZh3MJYg) PlanetProfile code is downloadable through Github (Vance, 2017). Salvus scripts are available upon request and require an active license to run.

Acknowledgements

A part of the research was carried out at the Jet Propulsion Laboratory, California Institute of Technology, under a contract with the National Aeronautics and Space Administration (80NM0018D0004). Work by JPL authors was supported by a grant from NASA's Habitable Worlds program (16-HW16 2-0065). Copyright 2022. We thank two anonymous reviewers for their thorough and helpful remarks.

References

Afanasiev, M., Boehm, C., van Driel, M., Krischer, L., Rietmann, M., May, D.A., Knepley, M.G., Fichtner, A., 2019. Modular and flexible spectral-element wave-form modelling in two and three dimensions. Geophys. J. Int. 216, 1675–1692. https://doi.org/10.1093/gji/ggy469.

Barnes, J.W., Turtle, E.P., Trainer, M.G., Lorenz, R.D., MacKenzie, S.M., Brinckerhoff, W.B., Cable, M.L., Ernst, C.M., Freissinet, C., Hand, K.P., Hayes, A.G., Hörst, S.M., Johnson, J.R., Karkoschka, E., Lawrence, D.J., Le Gall, A., Lora, J.M., McKay, C.P., Miller, R.S., Murchie, S.L., Neish, C.D., Newman, C.E., Núñez, J., Panning, M.P., Parsons, A.M., Peplowski, P.N., Quick, L.C., Radebaugh, J., Rafkin, S.C.R., Shiraishi, H., Soderblom, J.M., Sotzen, K.S., Stickle, A.M., Stofan, E.R., Szopa, C., Tokano, T., Wagner, T., Wilson, C., Yingst, R.A., Zacny, K., Stähler, S.C., 2021. Science goals and objectives for the dragonfly Titan rotorcraft relocatable lander. Planet. Sci. J. 2, 130. https://doi.org/10.3847/PSJ/abfdcf. https://iopscience.iop.org/article/10.3847/PSJ/abfdcf.

Běhounková, M., Souček, O., Hron, J., Čadek, O., 2017. Plume activity and tidal deformation on Enceladus influenced by faults and variable ice shell thickness. Astrobiology 17, 941–954. https://doi.org/10.1089/ast.2016.1629.

Beuthe, M., 2018. Enceladus's crust as a non-uniform thin shell: I tidal deformations. Icarus 302, 145–174. https://doi.org/10.1016/J.ICARUS.2017.11.009.

Čadek, O., Souček, O., Běhounková, M., Choblet, G., Tobie, G., Hron, J., 2019. Long-term stability of Enceladus' uneven ice shell. Icarus 319, 476–484. https://doi.org/10.1016/j.icarus.2018.10.003.

Čadek, O., Tobie, G., Van Hoolst, T., Massé, M., Choblet, G., Lefèvre, A., Mitri, G., Baland, R., Běhounková, M., Bourgeois, O., 2016. Enceladus's internal ocean and ice shell constrained from Cassini gravity, shape, and libration data. Geophys. Res. Lett. 43, 5653–5660. https://doi.org/10.1002/2016GL068634.

Choblet, G., Tobie, G., Sotin, C., Běhounková, M., Čadek, O., Postberg, F., Souček, O., 2017. Powering prolonged hydrothermal activity inside Enceladus. Nat. Astron. 1, 841–847. https://doi.org/10.1038/s41550-017-0289-8.

Collins, G.C., Patterson, G.W., Detelich, C.E., Prockter, L.M., Kattenhorn, S.A., Cooper, C.M., Rhoden, A.R., Cutler, B.B., Oldrid, S.R., Perkins, R.P., Rezza, C.A., 2022. Episodic plate tectonics on Europa: evidence for widespread patches of mobile-lid behavior in the antijovian hemisphere. J. Geophys. Res., Planets 127. https://doi.org/10.1029/2022je007492.

Crary, A.P., 1954. Seismic studies on Fletcher's ice island, T-3. Trans. Am. Geophys. Union 35, 293. https://doi.org/10.1029/TR035i002p00293.

Hand, K.P., Murray, A.E., Garvin, J.B., Brinckerhoff, W.B., Christner, B.C., Edgett, K.S., Ehlmann, B.L., German, C.R., Hayes, A.G., Hoehler, T.M., Horst, S.M., Lunine, J.I., Nealson, K.H., Paranicas, C., Schmidt, B.E., Smith, D.E., Rhoden, A.R., Russell, M.J., Templeton, A.S., Willis, P.A., Yingst, R.A., Phillips, C.B., Cable, M.L., Craft, K.L., Hofmann, A.E., Nordheim, T.A., Pappalardo, R.T., Team, P.E., 2017. Report of the Europa Science Definition Team. Technical Report. https://europa.nasa.gov/resources/58/europa-lander-study-2016-report/.

Hendrix, A.R., Hurford, T.A., Barge, L.M., Bland, M.T., Bowman, J.S., Brinckerhoff, W., Buratti, B.J., Cable, M.L., Castillo-Rogez, J., Collins, G.C., Diniega, S., German, C.R., Hayes, A.G., Hoehler, T., Hosseini, S., Howett, C.J.A., McEwen, A.S., Neish, C.D., Neveu, M., Nordheim, T.A., Patterson, G.W., Patthoff, D.A., Phillips, C., Rhoden, A., Schmidt, B.E., Singer, K.N., Soderblom, J.M., Vance, S.D., 2018. The NASA roadmap to ocean worlds. Astrobiology 19, 1–27. https://doi.org/10.1089/ast.2018.1955.

Hurford, T.A., Henning, W., Maguire, R., Lekic, V., Schmerr, N.C., Panning, M.P., Bray, V., Manga, M., Kattenhorn, S., Quick, L., Rhoden, A., 2020. Seismicity on tidally active solid-surface worlds. Icarus 338, 113466. https://doi.org/10.1016/j.icarus.2019.113466.

Iess, L., Stevenson, D.J., Parisi, M., Hemingway, D., Jacobson, R.A., Lunine, J.I., Nimmo, F., Armstrong, J.W., Asmar, S.W., Ducci, M., Tortora, P., 2014. The gravity field and interior structure of Enceladus. Science 344, 78–80. https://doi.org/10.1126/science.1250551.

Journaux, B., Brown, J.M., Pakhomova, A., Collings, I.E., Petitgirard, S., Espinoza, P., Boffa Ballaran, T., Vance, S.D., Ott, J., Cova, F., Garbarino, G., Hanfland, M., 2020. Holistic approach for studying planetary hydrospheres: Gibbs representation of ices thermodynamics, elasticity, and the water phase diagram to 2,300 MPa. J. Geophys. Res., Planets 125, e2019JE006176. https://doi.org/10.1029/2019JE006176.

Kovach, R.L., Chyba, C.F., 2001. Seismic detectability of a subsurface ocean on Europa. Icarus 150, 279–287. https://doi.org/10.1006/icar.2000.6577.

Lee, S., Zanolin, M., Thode, A.M., Pappalardo, R.T., Makris, N.C., 2003. Probing Europa's interior with natural sound sources. Icarus 165, 144–167. https://doi.org/10.1016/S0019-1035(03)00150-7.

Lognonné, P., Banerdt, W.B., Giardini, D., Pike, W.T., Christensen, U., Laudet, P., de Raucourt, S., Zweifel, P., Calcutt, S., Bierwirth, M., Hurst, K.J., Ijpelaan, F., Umland, J.W., Llorca-Cejudo, R., Larson, S.A., Garcia, R.F., Kedar, S., Knapmeyer-Endrun, B., Mimoun, D., Mocquet, A., Panning, M.P., Weber, R., Sylvestre-Baron, A., Pont, G., Verdier, N., Kerjean, L., Facto, L.J., Gharakanian, V., Feldman, J.E., Hoffman, T.L., Klein, D.B., Klein, K., Onufer, N.P., Paredes-Garcia, J., Petkov, M.P., Willis, J.R., Smrekar, S.E., Drilleau, M., Gabsi, T., Nebut, T., Robert, O., Tillier, S., Moreau, C., Parise, M., Aveni, G., Ben Charef, S., Bennour, Y., Camus, T., Dandonneau, P.A., Desfoux, C., Lecomte, B., Pot, O., Revuz, P., Mance, D., TenPierick, J., Bowles, N.E., Charalambous, C., Delahunty, A.K., Hurley, J., Irshad, R., Liu, H., Mukherjee, A.G., Standley, I.M., Stott, A.E., Temple, J., Warren, T., Eberhardt, M., Kramer, A., Kühne, W., Miettinen, E.P., Monecke, M., Aicardi, C., André, M., Baroukh, J., Borrien, A., Bouisset, A., Boutte, P., Brethomé, K., Brysbaert, C., Carlier, T., Deleuze, M., Desmarres, J.M., Dilhan, D., Doucet, C., Faye, D., Faye-Refalo, N., Gonzalez, R., Imbert, C., Larigauderie, C., Locatelli, E., Luno, L., Meyer, J.R., Mialhe, F., Mouret, J.M., Nonon, M., Pahn, Y., Paillet, A., Pasquier, P., Perez, G., Perez, R., Perrin, L., Pouilloux, B., Rosak, A., Savin de Larclause, I., Sicre, J., Sodki, M., Toulemont, N., Vella, B., Yana, C., Alibay, F., Avalos, O.M., Balzer, M.A., Bhandari, P., Blanco, E., Bone, B.D., Bousman, J.C., Bruneau, P., Calef, F.J., Calvet, R.J., D'Agostino, S.A., de los Santos, G., Deen, R.G., Denise, R.W., Ervin, J., Ferraro, N.W., Gengl, H.E., Grinblat, F., Hernandez, D., Hetzel, M., Johnson, M.E., Khachikyan, L., Lin, J.Y., Madzunkov, S.M., Marshall, S.L., Mikellides, I.G., Miller, E.A., Raff, W., Singer, J.E., Sunday, C.M., Villalvazo, J.F., Wallace, M.C., Banfield, D., Rodriguez-Manfredi, J.A., Russell, C.T., Trebi-Ollennu, A., Maki, J.N., Beucler, E., Böse, M., Bonjour, C., Berenguer, J.L., Ceylan, S., Clinton, J., Conejero, V., Daubar, I., Dehant, V., Delage, P., Euchner, F., Estève, I., Fayon, L., Ferraioli, L., Johnson, C.L., Gagnepain-Beyneix, J., Golombek, M., Khan, A., Kawamura, T., Kenda, B., Labrot, P., Murdoch, N., Pardo, C., Perrin, C., Pou, L., Sauron, A., Savoie, D., Stähler, S., Stutzmann, E., Teanby, N.A., Tromp, J., van Driel, M., Wieczorek, M., Widmer-Schnidrig, R., Wookey, J., 2019. SEIS: insight's seismic experiment for internal structure of Mars. Space Sci. Rev. 215, 12. https://doi.org/10.1007/s11214-018-0574-6.

Lucchetti, A., Pozzobon, R., Mazzarini, F., Cremonese, G., Massironi, M., 2017. Brittle ice shell thickness of Enceladus from fracture distribution analysis. Icarus 297, 252–264. https://doi.org/10.1016/j.icarus.2017.07.009.

Mackenzie, S.M., Neveu, M., Davila, A.F., Lunine, J.I., Craft, K.L., Cable, M.L., Phillips-lander, C.M., Hofgartner, J.D., Eigenbrode, J.L., Waite, J.H., Glein, C.R., Gold, R., Greenauer, P.J., Kirby, K., Bradburne, C., Kounaves, S.P., Malaska, M.J., Postberg, F., Patterson, G.W., Porco, C., Núñez, J.I., German, C., Huber, J.A., Mckay, C.P., Vera, J.p.D., Brucato, J.R., Spilker, L.J., 2021. The Enceladus orbilander mission concept: balancing return and resources in the search for life. Planet. Sci. J. 2, 77. https://doi.org/10.3847/PSJ/abe4da.

Maguire, R.R., Schmerr, N.C., Lekić, V., Hurford, T.A., Dai, L., Rhoden, A.R., 2021. Constraining Europa's ice shell thickness with fundamental mode surface wave dispersion. Icarus 369, 114617. https://doi.org/10.1016/j.icarus.2021.114617.

Marusiak, A.G., Panning, M.P., Vance, S.D., Nunn, C., Stähler, S.C., Tharimena, S., 2022a. Seismic detection of euroquakes originating from Europa's silicate interior. Earth Space Sci., 9. https://doi.org/10.1029/2021EA002041.

Marusiak, A.G., Vance, S., Panning, M.P., Bryant, A.S., Hesse, M.A., Carnahan, E., Journaux, B., 2022b. The effects of methane clathrates on the thermal and seismic profile of Titan's icy lithosphere. Planet. Sci. J. 3, 167. https://doi.org/10.3847/PSJ/ac787e.

Marusiak, A.G., Vance, S.D., Panning, M.P., Běhounková, M., Byrne, P.K., Choblet, G., Daswani, M.M., Hughson, K., Journaux, B., Lobo, A.H., Schmidt, B.E., Pleiner Sládková, K., Soderlund, K.M., Song, W., Souček, O., Steinbrügge, G., Thompson, A.F., Wang, S., 2021. Exploration of icy ocean worlds using geophysical approaches. Planet. Sci. J. 2, 150. https://doi.org/10.3847/PSJ/ac1272.

Masters, G., Woodhouses, J.H., Freeman, G., 2011. Mineos.

McKinnon, W.B., 2015. Effect of Enceladus's rapid synchronous spin on interpretation of Cassini gravity. Geophys. Res. Lett. 42, 2137–2143. https://doi.org/10.1002/2015GL063384.

National Academies of Sciences Engineering and Medicine, 2022. Origins, Worlds, and Life: A decadal Strategy for Planetary Science and Astrobiology 2023-2032. National Academies Press, Washington, D.C. https://www.nap.edu/catalog/26522.

Olgin, J.G., Smith-Konter, B.R., Pappalardo, R.T., 2011. Limits of Enceladus's ice shell thickness from tidally driven tiger stripe shear failure. Geophys. Res. Lett. 38. https://doi.org/10.1029/2010GL044950.

Panning, M.P., Lekic, V., Manga, M., Cammarano, F., Romanowicz, B., 2006. Long-period seismology on Europa: 2. Predicted seismic response. J. Geophys. Res., Planets 111. https://doi.org/10.1029/2006JE002712.

Panning, M.P., Stähler, S.C., Vance, S.D., Kedar, S., Tsai, V.C., Pike, W.T., Lorenz, R.D., Huang, H.H., Vance, S.D., Kedar, S., Tsai, V.C., Pike, W.T., Lorenz, R.D., 2018. Expected seismicity and the seismic noise environment of Europa. J. Geophys. Res., Planets 123, 163–179. https://doi.org/10.1002/2017JE005332.

Pappalardo, R.T., Vance, S.D., Bagenal, F., Bills, B.G., Blaney, D.L., Blankenship, D.D., Brinckerhoff, W.B., Connerney, J.E., Hand, K.P., Hoehler, T.M., Leisner, J.S., Kurth, W.S., McGrath, M.A., Mellon, M.T., Moore, J.M., Patterson, G.W., Prockter, L.M., Senske, D.A., Schmidt, B.E., Shock, E.L., Smith, D.E., Soderlund, K.M., 2013. Science potential from a Europa lander. Astrobiology 13, 740–773. https://doi.org/10.1089/ast.2013.1003.

Stähler, S.C., Panning, M.P., Vance, S.D., Lorenz, R.D., van Driel, M., Nissen-Meyer, T., Kedar, S., Driel , M.v., Nissen-Meyer, T., Kedar, S., 2017. Seismic wave propagation in icy ocean worlds. J. Geophys. Res., Planets 123, 206–232. https://doi.org/10.1002/2017JE005338.

Tajeddine, R., Soderlund, K.M., Thomas, P.C., Helfenstein, P., Hedman, M.M., Burns, J.A., Schenk, P.M., 2017. True polar wander of Enceladus from topographic data. Icarus 295, 46–60. https://doi.org/10.1016/j.icarus.2017.04.019.

Vance, S., 2017. vancesteven/planetprofile: Release for use in reproducing results submitted to Journal of Geophysical Research: Planets. Zenodo.

Vance, S.D., Behounkova, M., Bills, B.G., Byrne, P., Cadek, O., Castillo-Rogez, J., Choblet, G., Hughson, K., Hurford, T., Kedar, S., Keane, J., Kite, E., Lobo, A.H.,

Marusiak, A.G., Daswani, M.M., Panning, M.P., Park, R.S., Schmidt, B.E., Sladkova, K., Soderlund, K.M., Sotin, C., Soucek, O., Stähler, S., Steinbrügge, G., Tharimena, S., Thompson, A., Tobie, G., Song, W., Wang, S., 2021a. Distributed geophysical exploration of Enceladus and other ocean worlds. Bull. Am. Astron. Soc. 53, 127. https://doi.org/10.3847/25c2cfeb.a07234f4.

Vance, S.D., DellaGiustina, D.N., Hughson, K., Hurford, T., Kedar, S., Marusiak, A.G., Melwani Daswani, M., Panning, M.P., Schmerr, N.C., Schmidt, B.E., Stähler, S., Tharimena, S., Tobie, G., Weber, R.C., 2021b. Planetary seismology: the solar system's ocean worlds. In: Bulletin of the American Astronomical Society, p. 129. https://ui.adsabs.harvard.edu/abs/2021BAAS...53d.129V.

Vance, S.D., Marusiak, A.G., Daswani, M.M., Styczinski, M.J., Lisitsyn, A., Vega, K., Bryant, A., 2022. PlanetProfile: supplementary data: effects of methane clathrate lids on Titan's ice shell and added TauP functionality. https://doi.org/10.5281/zenodo.6323610.

Vance, S.D., Panning, M.P., Stähler, S., Cammarano, F., Bills, B.G., Tobie, G., Kamata, S., Kedar, S., Sotin, C., Pike, W.T., Lorenz, R.D., Huang, H.H.H., Jackson, J.M., Banerdt, B., 2018. Geophysical investigations of habitability in ice-covered ocean worlds. J. Geophys. Res., Planets 123, 180–205. https://doi.org/10.1002/2017JE005341.

Waite, J.H., Glein, C.R., Perryman, R.S., Teolis, B.D., Magee, B.A., Miller, G., Grimes, J., Perry, M.E., Miller, K.E., Bouquet, A., Lunine, J.I., Brockwell, T., Bolton, S.J., 2017. Cassini finds molecular hydrogen in the Enceladus plume: evidence for hydrothermal processes. Science 356, 155–159. https://doi.org/10.1126/science.aai8703.